

# Narrowing the Photoluminescence of Aqueous CdTe Quantum Dots via Ostwald Ripening Suppression Realized by Programmed Dropwise Precursor Addition

Xiaodan Huang,<sup>†,‡</sup> Lihong Jing,<sup>\*,†,‡</sup> Stephen V. Kershaw,<sup>§</sup> Xiaojun Wei,<sup>†,‡</sup> Haoran Ning,<sup>†,‡</sup> Xiaodan Sun,<sup>†,‡</sup> Andrey L. Rogach,<sup>\*,§</sup> and Mingyuan Gao,<sup>\*,†,‡</sup>

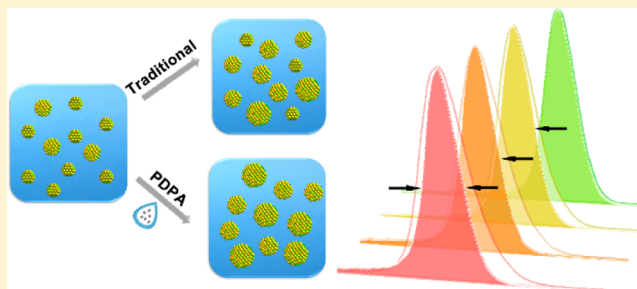
<sup>†</sup>Key Laboratory of Colloid, Interface and Chemical Thermodynamics, Institute of Chemistry, Chinese Academy of Sciences, Bei Yi Jie 2, Zhong Guan Cun, Beijing 100190, China

<sup>‡</sup>School of Chemistry and Chemical Engineering, University of Chinese Academy of Sciences, Beijing 100049, China

<sup>§</sup>Department of Materials Science and Engineering & Centre for Functional Photonics, City University of Hong Kong, 83 Tat Chee Avenue, Kowloon, Hong Kong S. A. R, China

## Supporting Information

**ABSTRACT:** Ostwald ripening is the dominant particle growth mechanism in traditional routes to synthesize aqueous CdTe quantum dots (QDs), which results in a broadening of their size distribution and also their photoluminescence line width, in the case of prolonged reactions. We introduce a method to suppress the Ostwald ripening through the replenishment of precursors before size defocusing occurs in the aqueous synthetic system, which is realized through a programmed dropwise precursor (source) addition (denoted as PDPA) by a syringe pump arrangement that can control the precursor feed volume and rate. As a result, we have obtained a series of highly monodisperse CdTe QDs, with the emission full width at half-maximum in the red region (106 meV) being even narrower than that in the green region (160 meV). We monitored the conductivity of the reaction solution to follow the consumption of precursors, providing feedback as to whether the replenishment volume was matched. Correlations between the emission quantum yield and the fluorescence lifetime for different precursor source addition rates are provided. The influence of the respective sizes of the CdTe particles employed as precursors in PDPA on the growth rate, monodispersity, and emission characteristics of the resulting QDs is explored, and the underlying mechanisms are rationalized.



## INTRODUCTION

Because of their outstanding light-emitting properties and convenient synthesis methods, semiconductor quantum dots (QDs) have shown great potentials for both optoelectronic devices<sup>1–3</sup> and biomedical labeling.<sup>4–10</sup> One well-established way to prepare II–VI QDs is to employ aqueous synthesis, with CdTe QDs being a prominent example.<sup>11–14</sup> The rich choice of thiol surface ligands available for aqueous synthetic routes allows easy tailoring of QDs toward specific applications, such as biolabeling,<sup>15–19</sup> self-assembly,<sup>20,21</sup> and optical chirality.<sup>22–24</sup> For applications in biolabeling, light-emitting devices and displays achieving narrow size distributions of the QDs are of particular importance, as they control the emission color and color purity. However, the photoluminescence (PL) peaks of QDs prepared through aqueous synthetic routes often become progressively broader as emission is shifted toward the red region, as the particle growth mechanism is dominantly governed by Ostwald ripening. One commonly used way to improve the monodispersity of the QD products is to employ postpreparative size-selective precipitation,<sup>11,13,25</sup> which is, however, a time-consuming process where the reproducibility

of the resulting particle batches is hard to guarantee. As an alternative, hydrothermal syntheses were developed, where increased reaction temperature helped to achieve the size-focusing stage.<sup>26,27</sup> As a result, narrower particle size distributions were obtained for CdTe QDs, with the full width at half-maximum (fwhm) of the PL peaks reduced from 170–200 meV, typical for the “traditional” aqueous synthetic routes, down to 140–160 meV in the red region. Microwave heating method allowed the production of CdTe QDs with an fwhm of 111 meV for green-emitting QDs, but the PL peaks still experienced broadening upon shifting toward the red spectral region because of Ostwald ripening.<sup>28</sup> 3-Mercaptopropionic acid is a widely used ligand allowing the growth of larger CdTe QDs,<sup>29</sup> but again because of the Ostwald ripening constraints, the fwhm of the PL peaks is rather broad (about 240 meV) in the red-to-near-infrared (NIR) region.<sup>30</sup> Yang and co-workers reported QD-cellulose composites with an fwhm of

Received: January 30, 2018

Revised: May 2, 2018

Published: May 2, 2018

132 meV for the PL at 680 nm; by utilizing an elongated light path in their detection system and taking advantage of reabsorption, they realized a PL peak with an fwhm of 94 meV in the red region, but the innate particle size distribution still remained broad.<sup>31</sup>

These studies illustrate the critical point related to most of the traditional aqueous synthesis methods: an intrinsic trend of broadening the emission spectra in the later stages of the particle growth due to the Ostwald ripening and the related difficulty to realize monodisperse size distributions in the resulting QDs. The aqueous synthesis of semiconductor nanocrystals (NCs) is essentially a precipitation reaction, which occurs under participation of cationic and anionic precursors in the presence of ligand(s). Ligands are stabilizing agents which are essential to control the precipitation process during the early stage so as to limit the growth of nanoparticles, rather than proceeding to bulklike precipitates. Cationic and anionic precursors can be considered as “precursors” that react quickly in the aqueous phase when their concentration exceeds a critical level, which is known as the nucleation threshold. After reaching this stage, the particle growth will quickly transition into the Ostwald ripening regime, especially at elevated temperatures. The precursors are consumed, their concentration decreases to a certain level, and thereafter defocusing of the size distribution occurs. In traditional aqueous syntheses,<sup>2</sup> QDs grow rather slowly so that the emission of CdTe QDs, as an example, shifts from green to red or NIR over the course of tens to hundreds of hours. As in the classical Ostwald ripening regime, larger QDs grow in size whilst smaller particles shrink in size and eventually disappear, and in the process, they furnish an additional source of precursors for the further enlargement of the larger particles. During this process, the particle size distribution becomes broader; this inevitably results in the PL peaks suffering from progressive broadening during the prolonged QD growth.

In nonaqueous syntheses such as organometallic routes and thermal decomposition methods,<sup>32–34</sup> metal–organic precursors decompose and react under diffusion control and, as a consequence, the particle size distribution of the QDs can become narrower during the growth, which has been denoted as the “size-focusing regime”.<sup>35</sup> Each precursor concentration corresponds to a critical size. If the critical size is smaller than those of all NCs in solution, focusing of the size distribution occurs, as the smaller NCs grow faster than the large ones. However, the precursor concentration is rapidly depleted on a time scale of minutes, so a second injection of molecular precursors is to be carried out so that the follow-on into Ostwald ripening is prevented. Later on, this method was further refined by Bawendi et al.<sup>36</sup> who decoupled the nucleation and growth stages in the process of synthesizing InAs QDs, exerting control by continuously injecting further volumes of arsenic precursors, which successfully narrowed the QD size distribution. Jeong et al.<sup>37</sup> controlled the size distribution of InAs QDs via injecting amorphous prenucleated clusters instead of the molecular precursors as the precursor source. These approaches are now well-established in nonaqueous QD syntheses and have resulted in significantly improved size distribution control and, as a result, in the narrow emission peaks of the resulting II–VI and III–V nanoparticles.

By taking advantage of these approaches, which have been developed already for the nonaqueous synthetic routes, we have developed a methodology to forestall the Ostwald ripening

process in the aqueous synthesis system, aiming at the replenishment of the precursors before size defocusing starts to occur. We have achieved this using a programmable syringe pump which can control the supplying rates of the precursor source, which we denote as programmed dropwise precursor addition (PDPA) method. We have employed conductivity measurement on the reaction mixture to monitor the consumption of the precursors during the course of reaction and thus to determine appropriate precursor addition volumes and rates. Using the PDPA method, we have obtained a series of CdTe QDs with a broad range of emission wavelengths with significantly better monodispersity than that in the traditional synthetic method, where PL fwhms in the red region (106 meV) were even narrower than those in the green region (160 meV). Finally, we conducted a number of syntheses employing not only precursors but also presynthesized CdTe seeds (the QD solutions to which the precursor source QDs were added) produced using different Te precursors, which led to some notable differences in the ensuing growth kinetics. These studies allowed us to determine how to achieve the best match for the sizes of seeds and provided additional insights into the growth mechanisms and size focusing.

## ■ EXPERIMENTAL SECTION

**Chemicals.** Cadmium perchlorate hexahydrate ( $\text{Cd}(\text{ClO}_4)_2 \cdot 6\text{H}_2\text{O}$ ) (Aldrich, 99.9%), cadmium acetate dihydrate ( $\text{Cd}(\text{CH}_3\text{COO})_2 \cdot 2\text{H}_2\text{O}$ ) (Aladdin, AR), thioglycolic acid (TGA) (Fluka, 97%+), aluminum telluride ( $\text{Al}_2\text{Te}_3$ ) (CERAC Inc., 99.5%), sodium tellurite ( $\text{Na}_2\text{TeO}_3$ ) (Aladdin, 97%), and sodium borohydride ( $\text{NaBH}_4$ ) (Sinopharm Chemical Reagent Co., Ltd, 98%) were all used as received.

**Instruments.** A programmable syringe pump (Longer TJP-3A, with a 20 or 60 mL injection syringe) and a conductivity meter (Jenway 4320 Bench Conductivity/TDS Meter) were used.

**Synthesis of CdTe QD Seeds by the Traditional Method.** CdTe QDs stabilized by TGA were synthesized by introducing  $\text{H}_2\text{Te}$  (formed upon the reaction between  $\text{Al}_2\text{Te}_3$  and 0.5 M diluted sulfuric acid) into an aqueous solution containing  $\text{Cd}^{2+}$  and TGA at pH 12.0 under nitrogen protection for 30 min.<sup>38–40</sup> The feeding ratio of Cd/Te/TGA was set to 1:0.58:1.3. Thereafter, the resulting reaction mixture was immediately refluxed under open-air conditions to generate CdTe QDs with desired sizes according to the refluxing time. By this method, we obtained red fluorescent QDs as seeds to participate in the next steps.

**Synthesis of CdTe QDs by the PDPA Method.** Additional QD precursors (or more accurately different sized QDs that act as a source of precursors) were introduced into the above as-prepared CdTe QD seeds by a programmable syringe pump that allows control of the precursor feed volume and rate. To differentiate these from the starting seeds, all additional precursors for the PDPA method are denoted as precursors or “sources of precursors”, even though they have already been grown into NCs. These (sources of) precursors were prepared using a mixture of  $\text{Cd}^{2+}/\text{TGA}/\text{TeO}_3^{2-}$  in a ratio of 1:1.3:0.2 at pH 12.0. In detail, 0.533 g (2 mmol) of  $\text{Cd}(\text{CH}_3\text{COO})_2 \cdot 2\text{H}_2\text{O}$  was dissolved in 50 mL of water, and 0.259 g (2.6 mmol) of TGA was added under stirring, followed by adjusting the pH value to 12.0 by dropwise addition of a 1 M solution of NaOH. After stirring for 5 min, 0.0890 g (0.4 mmol) of  $\text{Na}_2\text{TeO}_3$  which was dissolved in 50 mL of deionized water was added. Then, 0.400 g of  $\text{NaBH}_4$  was added into the

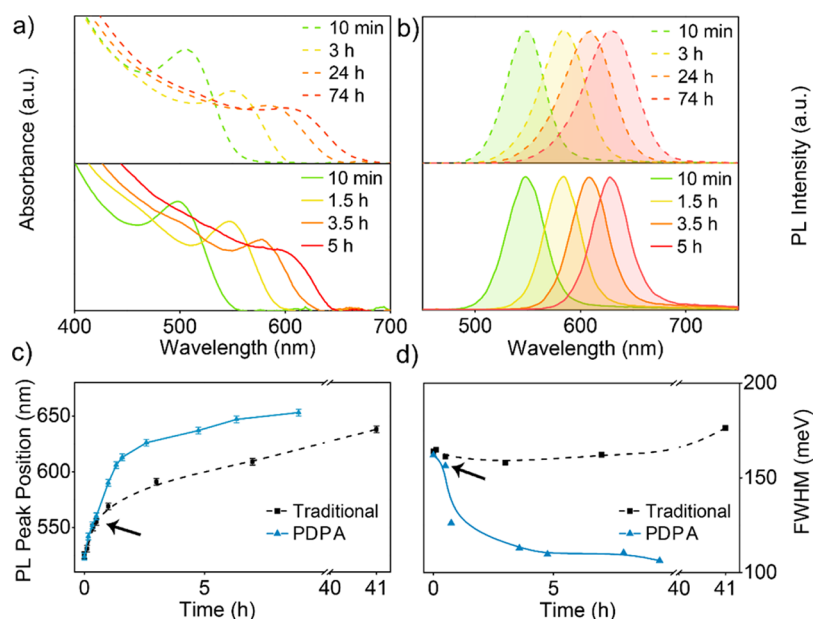


**Figure 1.** Temporal evolution of (a) absorption and (b) PL spectra of CdTe QDs obtained via traditional aqueous synthesis (dashed lines) and the PDPA method (solid lines). Temporal evolution of (c) PL peak positions and (d) PL fwhm of CdTe QDs obtained via traditional method (black squares) and PDPA method (blue triangles). The black arrows in (c,d) indicate the PDPA starting point.

solution before deaeration by bubbling with  $N_2$  for 0.5 h. Additionally, to obtain precursor QDs with a range of different sizes, as shown in later discussion, the precursor solutions were heated under reflux for various time periods before introducing into the seeds.

**Control Experiments.** In order to explore the effects of different combinations of CdTe seeds and precursors obtained by varying types of Te precursors on the PL fwhms in the PDPA method, additional experiments were carried out in the following. In the above typical PDPA experiment, we use  $H_2Te$  as the  $Te^{2-}$  source to synthesize QDs as starting seeds, and then  $Na_2TeO_3$  as the Te source to supply precursors for replenishment during PDPA growth. Compared to the typical PDPA experiment, in one control experiment, additional precursors were supplied by  $H_2Te$  precursor-derived QDs instead of those formed using  $TeO_3^{2-}$ , whereas in another control experiment, conversely, the starting seeds were synthesized using  $Na_2TeO_3$  instead of  $H_2Te$ .

**Structural Characterization.** Transmission electron microscopy (TEM) images were recorded on a HT7700 microscope. High-resolution TEM (HRTEM) images were recorded on a JEM-2100F microscope after a calibration using thin Au film. To improve the imaging contrast, QDs were transferred from water into toluene by utilizing octadecyl-*p*-vinylbenzyl-dimethylammonium chloride as a phase-transfer agent to avoid particle aggregation on the carbon supporting film of TEM copper grids.<sup>41</sup>

**Spectroscopic Characterization.** Steady-state UV–vis absorption and PL spectra were recorded at room temperature on a Cary 50 UV–vis spectrophotometer and a Cary Eclipse fluorescence spectrophotometer, respectively. The excitation wavelength for all steady-state PL measurements was set to 400 nm. The PL quantum yield (QY) of QDs was estimated by using rhodamine 6G as a fluorescence standard according to a literature method.<sup>14</sup> Time-resolved PL decay measurements were carried out on an Edinburgh Instruments FLS980 spectrometer equipped with a picosecond pulsed diode laser (EPL-405 nm, pulse width: 49 ps) as a single-wavelength

excitation source (405 nm) for time-correlated single-photon counting measurements.

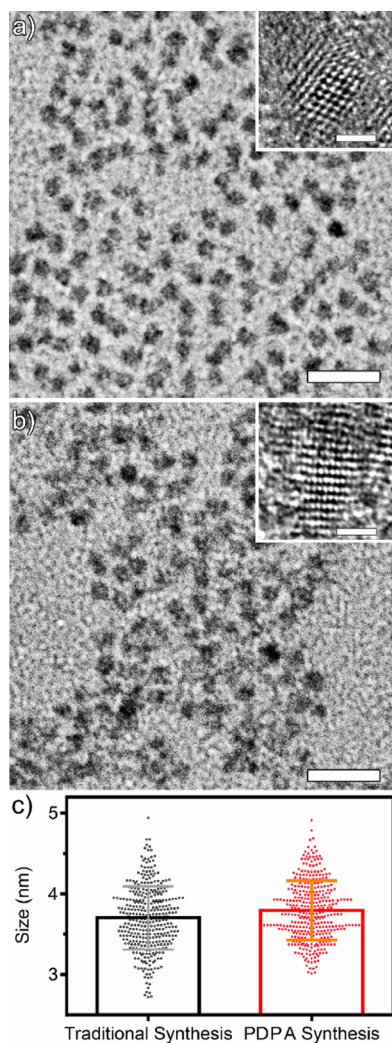
## RESULTS AND DISCUSSION

### Restraining Ostwald Ripening via the PDPA Method.

In the traditional aqueous synthesis method for TGA-capped CdTe QDs, the solution of precursors is refluxed at 100 °C under open-air conditions for up to 75 h. When employing the PDPA method, the reaction kinetics can be significantly accelerated in comparison with that in the traditional method, as illustrated by temporal evolutions of the absorption spectra, PL spectra, and corresponding peak positions shown in Figure 1a–c. In the traditional aqueous synthesis, PL spectra exhibit an obvious broadening as the growth progressed into the red region, as shown in Figure 1b (dashed line), whereas for the PDPA method, this tendency is reversed. As shown in Figure 1d, as the duration of the reaction increased, the fwhms of the PL peaks increased to nearly 180 meV at 640 nm in the traditional synthesis. In terms of the ratio, fwhm/peak wavelength, the widths were 6.9% and 8.8% in the green and red regions, respectively. In the traditional synthesis, the growth rate slowed a lot after about half an hour, meaning that the precursors were almost fully depleted by that point, with the focusing stage coming to an end. Therefore, we chose 1 h as the start for the injecting point for the subsequent PDPA. Initially, 50 mL of CdTe QD precursor were reacted for 1 h by which time the solution had a green-yellow fluorescence with a 560 nm PL peak. Then, 20 mL of the QD precursor source solution was slowly injected into the reaction liquid by the injection pump over the course of an hour. During this time, the PL peak shifted rapidly from 560 to 590 nm, while the PL fwhm decreased from 156 to 126 meV (Figure 1c,d, respectively). In terms of the ratio of fwhm/PL peak wavelength, the change represents a drop from 7% to 6%. This shows that controlling the precursor concentration can restrain the Ostwald ripening process, accelerate the particle growth, and narrow down the PL fwhm of the resulting CdTe QDs. However, introducing a

large excess of precursor QDs may deteriorate the PL QY of the QDs; we will address this issue in the following section.

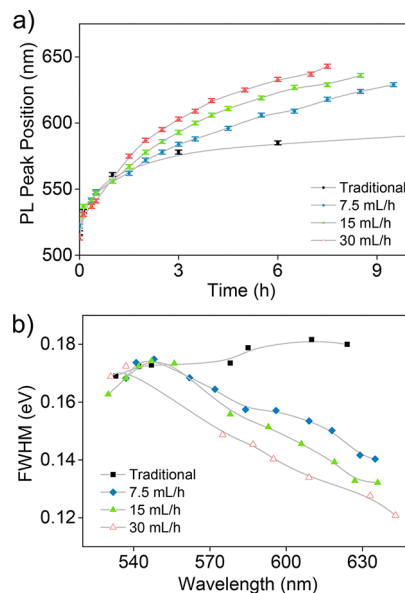
Representative TEM and HRTEM images of CdTe QDs obtained by the traditional and PDPA synthesis groups together with their particle size distribution profiles are shown in Figure 2a,b, respectively. Whereas the average sizes are rather similar at 3.7 and 3.8 nm, the particle size distribution narrowed in the PDPA case, as seen in Figures 2c and S1.



**Figure 2.** TEM and HRTEM images of CdTe QDs obtained via (a) traditional synthesis method and (b) via PDPA method, together with (c) deviations of particle sizes from the average size estimated from TEM. The scale bars in the TEM and HRTEM images correspond to 20 and 2 nm, respectively.

**Influence of the PDPA Rate on Growth Rate and PL fwhm Variation.** In order to study how different PDPA rates influence particle growth, we further investigated several different addition strategies. The most successful approach was an iterative or interval injection protocol, as it resulted in the narrow PL fwhm mentioned in the previous section and, at the same time, could also retain the high PL QY of the traditional synthesis method. We set up three groups of syntheses with different PDPA rates, all of which used a 1 min QD precursor source addition and 1 min pause over a number of cycles. The PDPA volumes for each set were 0.25, 0.50, and 1.00 mL per cycle, which meant averaged addition rates of 7.5,

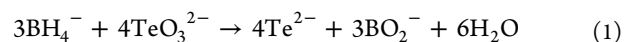
15, and 30 mL/h, respectively. As shown in Figure 3, compared with the traditional synthesis, each PDPA case was faster in



**Figure 3.** Temporal evolution of (a) PL peak positions and (b) PL fwhm of CdTe QDs obtained from the PDPA method while employing different injection rates of 7.5, 15, and 30 mL/h, as indicated on the frames. Comparison with the traditional synthesis (black squares) is also given.

terms of the PL peak red shift and narrower in terms of PL fwhm. The increase in PDPA rate results in an increase of the QD growth and in a decrease of the PL fwhms. This trend can be rationalized within the size-focusing mechanism. As a result of the injection of additional precursors, the total precursor concentration becomes higher than what would be provided by the redissolution not only of big particles but also of small particles in the ensemble, and this would promote the growth of all particles across their whole size distribution. Under these conditions, diffusion-controlled growth prevails whereby the volume of every particle increases at the same rate,<sup>35,42</sup> meaning that smaller particles would grow faster than larger ones, which leads to size focusing in the end. Higher PDPA rates lead to higher concentration gradients around QDs realized after each addition, which increases the precursor diffusion rate toward the QD surface, accelerating the growth rate and promoting the focusing of the size distribution.

**Monitoring the Consumption of Precursors via Conductivity Changes during the Ongoing PDPA Reaction.** Even though it is hard to develop a reliable assay for the many constituents present in the reaction environment during the aqueous synthesis of QDs, we chose on-line monitoring of the solution conductivity as a measure of the effective ionic mobility to follow the ongoing PDPA reactions process, especially after the addition of the QD precursors. Bearing in mind that the mobility of the small free ionic precursors would be higher than that of the charged but much larger QDs, the conductivity is expected to be heavily weighted by the contributions from the precursors. For the tellurite-based precursor addition method, the precursors are consumed according to the following chemical reactions:<sup>43</sup>



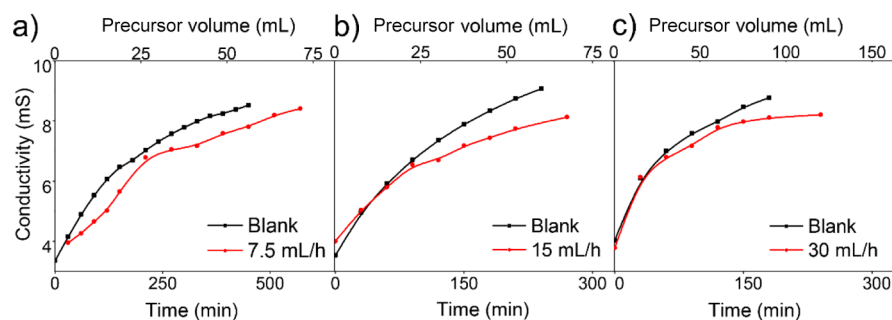


**Figure 4.** Temporal changes in conductivity for the blank group (black squares) and the reaction group (red dots) for three different QD precursor source injection rates of (a) 7.5, (b) 15, and (c) 30 mL/h in PDPA reactions.

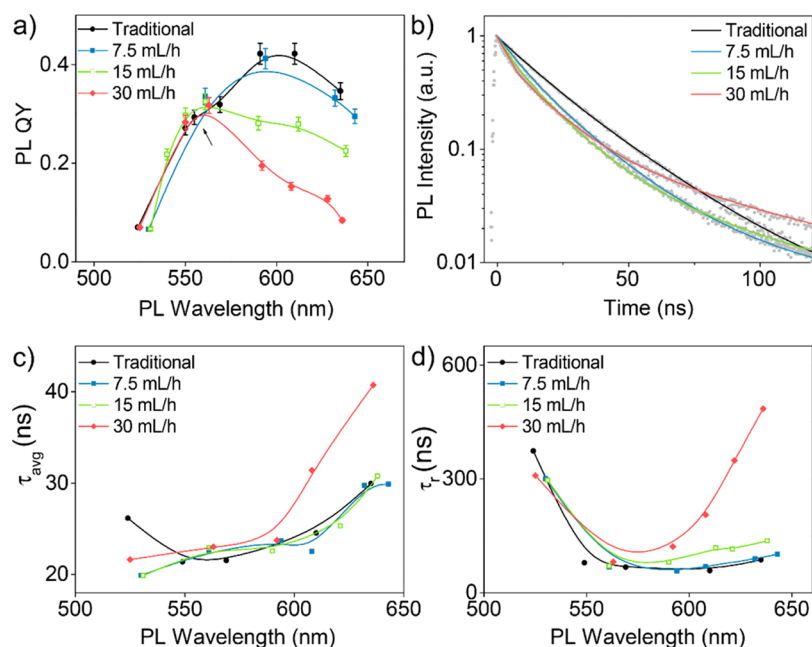
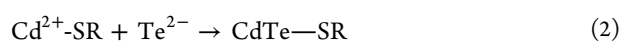


**Figure 5.** Influence of PDPA rate on (a) PL QY, (b) PL decay curves, (c) average PL lifetime ( $\tau_{\text{avg}}$ ), and (d) radiative recombination lifetime ( $\tau_r$ ) of CdTe QDs. Systematic error is approximately  $\pm 0.5$  ns for all lifetime values.



While freshly supplied  $\text{Te}^{2-}$  anions react with Cd-SR to form CdTe QDs capped by the thiol ligand SR, the conductivity should decline, giving the basis on which to monitor the precursor consumption via the conductivity measurements.

We followed the conductivity and the variations in the PL fwhm in the PDPA reaction as exemplified by the data shown in Figure S2. It was observed that after each addition of precursors, the conductivity of the solution rose and the PL fwhm of the QDs decreased. Each precursor injection introduced additional ions, leading to an increase of the conductivity. Once the addition was stopped, the conductivity descended and the fwhm increased again, as the diffusion-limited growth gave way to Ostwald ripening. The decrease in the solution conductivity has two main contributions: the first is the consumption of  $\text{Te}^{2-}$  as per reactions 1 and 2 and the second is the consumption of excess  $\text{NaBH}_4$ . Excess  $\text{NaBH}_4$  can react with  $\text{H}_2\text{O}$  or  $\text{O}_2$  in the system; this may result in the lower conductivity. In order to be able to judge which is the major contribution to the changes in the conductivity, either the borohydride side reactions or  $\text{Te}^{2-}$  depletion 1 and 2, the following blank experiment was conducted. NaOH solution at

pH 12.0 was prepared, and 0.80 g of  $\text{NaBH}_4$  was added to it and refluxed at 100 °C under open-air conditions with a condenser attached whilst the conductivity was monitored. The conductivity gradually declined over several hours, with a rate of 0.1 mS in every 30 min, lower than the rate of change under the QD reaction conditions (0.3–0.6 mS over similar intervals), as shown in Figure S2. This means that changes in the excess of  $\text{NaBH}_4$  contributed only a little part to the overall decline of conductivity as a slow background variation so that it is meaningful to monitor the consumption of precursors by measuring the conductivity change.

We then performed a series of conductivity measurements on a blank group and a synthesis group to compare the conductivity variation for three different PDPA injection rates (7.5, 15, and 30 mL/h) and to draw conclusions as to whether the precursors were exhausted for each of the cases. For the blank group, the same set of PDPA rates was used in order to follow the increase of conductivity in the nonreacting solutions where QD growth did not contribute to the removal of ionic materials. The overall increase in conductivity under reaction conditions for all three injection rates as compared to the same PDPA rates in the blank experiments is shown in Figure 4. For the slow PDPA injection rate (7.5 mL/h), the two curves

separated at the outset, with the lower synthesis batch conductivity indicating the effect of the precursor consumption. For both higher PDPA injection rates (15 and 30 mL/h), the two curves were almost coincident at the beginning of the reactions and separated afterward, which indicated that PDPA precursors were in excess and could not be consumed more rapidly than they were added.

**Influence of PDPA Rate on the Optical Properties of CdTe QDs.** The influence of the PDPA rate on the optical properties of CdTe QDs has been studied by PL QY and time-resolved PL measurements. Figure 5a shows the effect of various PDPA rates used in the precursor solution on the PL QY of the as-prepared CdTe NCs. Compared with the traditional group, adding precursors always reduced the PL QY to some extent. For the highest PDPA rate of 30 mL/h, the PL QY declined sharply once the injection was started (560 nm emission) and finally decreased to almost 10% for 640 nm emission samples. It appears that the influx of precursor source solution, which contains various kinds of ions and especially the strong reducing agent  $\text{NaBH}_4$ , influences the particle surface passivation and thus quenches the PL. For the case of 7.5 mL/h injection rate, the PL QY can be maintained much closer to the values measured for the traditional group. We conclude that there is an optimal precursor injection rate for the synthesis of high-quality QDs where the precursors can react completely to ensure size focusing on the one hand whilst the PL QY can be maintained at a high level on the other hand.

Figure 5b shows the representative PL decay curves (measured at a PL emission peak wavelength of 635 nm) of CdTe QDs as a function of precursor injection rate. Moreover, the PL lifetimes at the emission peaks of the shifting spectra during reaction process are shown in Figure 5c. The average decay lifetime in the PDPA group exhibited an enhanced injection rate-dependent behavior with reflux time, especially after the PL peak position increased to 590 nm, and the faster the injection speed, the longer the average decay lifetime. In contrast, the control (traditional synthesis) group showed similar average PL decay lifetimes across the wavelength range, again suggesting that the addition of precursors greatly increased the PL lifetimes, nearly doubling them from 19.9 to 40.7 ns for the 636 nm peak PL. In addition, the radiative recombination lifetime ( $\tau_r$ ) in Figure 5d shows that as the precursor addition proceeded, the radiative recombination lifetimes became longer in the injected group compared with the control group.

In our experiments, taking the PL peak at 630 nm as an example, the 7.5 mL/h group needed to continue the precursor addition for 10 h to add 75 mL of precursor solution to reach this wavelength. The 15 mL/h group needed 6.5 h, adding 97.5 mL of precursors, and the 30 mL/h group needed about 4.5 h to add 135 mL of precursors to bring about the same peak shifts. That is to say, although the PL peak positions (between groups) are similar, the total ionic concentrations both consumed and excess remaining in solution may differ significantly. It is also worth noting that where the growth is fueled by the addition of smaller QDs, the ratio of cations to anions in the injected feedstock QDs will reflect those for small QDs and not necessarily the ratio used in the traditional synthesis for example. According to the energy-dispersive spectrometry (EDS) data obtained on CdTe QD samples as presented in Figure S3, the relative ratio of Cd/Te and S/Te increases for the particles produced by the PDPA method as compared to those produced by the traditional method. Such a

tendency can be caused by better coordination of TGA ligands to  $\text{Cd}^{2+}$  in the PDPA method. This causes a drift in the QD stoichiometry because smaller QDs are generally known to be proportionately more cation-rich<sup>44–46</sup> and cause PDPA-enlarged QDs to be more cation-rich than they might naturally be when made by the traditional method. In other words, the PDPA group may tend to show a drift toward cation-to-anion ratios that would normally be seen in smaller QDs when synthesized by the traditional scheme. Although the QD size and ligand environment impact upon absorption and radiative emission rates have been investigated by many groups,<sup>44–46</sup> there is little mention of the impact of variation of (cation/anion) stoichiometry upon the transition rates (though of course similar studies upon the effect of cation ratios have been made in ternary systems).<sup>47,48</sup> There are three principle means by which the internal QD composition might influence absorption and emission radiative rates: changes in the local field factor, which will change the rate of coupling of photons between the QD and the local environment; formation of a heterostructure, which will change the spatial overlap between electrons and holes; or other perturbation of the overlap of the excited carriers. In the present case, when comparing QDs of similar sizes but with different effective cation/anion feed ratios, we postulate that they may have slightly different surface cation excesses. Both the emission and absorption rates show some sensitivity for larger QD sizes. Apart from the progressively longer radiative relaxation times with increasing total amounts of added precursor source, the strength of the band edge emission for larger QDs also seems to be proportionately weakened (as seen in the comparisons of short-wavelength normalized absorption spectra in Figure S4). The normalization with the optical densities at 400 nm takes account of the differing QD concentrations in the solutions, allowing relative comparisons between samples with the same (or near similar) QD sizes, that is, for materials with excitonic peaks at similar wavelengths. Evidently, both absorption and emission rates for larger PDPA-grown samples are lower than those for the traditionally synthesized material. One possible mechanism for this may be via a stoichiometry-dependent change in the local field factor (see the discussion in the Supporting Information below Figure S4). If we consider the QD as a stoichiometric core where the dielectric properties correspond to those of bulk CdTe (such as in ref 49), then the outermost shell would be an atomic layer of predominantly cadmium ion (Moreels et al. considered a similar case for Pb-coated stoichiometric PbSe QDs).<sup>50</sup> Of course, there is no literature data that provide the complex permittivity of the latter type of exclusively cationic shell. A crude approximation may be to take the values for Cd(0) from measurements on metallic Cd crystals<sup>51</sup> and calculate the effective local field factor using the expression for core shells given by Neeves and Birnboim,<sup>52,53</sup> for such an atomic surface layer, we estimated a change in the square of the field factor to be 0.1070 compared with 0.1179 for the stoichiometric case. Thus, it may be reasonable to expect up to a 10% change in the transition rates on such a basis. If the surface layer were also to contribute to preferentially localizing one or the other of the two excited carriers near the surface whilst repelling the other, this might also influence the transition rates by altering the wave function overlap term, further influencing the transition rates.

A more complete analysis of the effect of variations of stoichiometry on the optical and dielectric properties of the QDs might be accessible by tight binding<sup>54</sup> or other atomistic

modeling approaches,<sup>55</sup> but that remains beyond the scope of this work.

**PDPA Syntheses Conducted with Different Precursor and Seed Combinations.** In all experiments presented above, we used  $\text{H}_2\text{Te}$  as the Te source to synthesize green fluorescent QDs as seeds and  $\text{Na}_2\text{TeO}_3$  as the Te source to synthesize PDPA precursors for replenishment during growth. We have also explored other seed and precursor combinations as control experiments as follows. The absorption spectra of the two different seeds, CdTe seeds obtained by the  $\text{H}_2\text{Te}$  precursor and  $\text{Na}_2\text{TeO}_3$  precursor, are shown in Figure 6a. The  $\text{H}_2\text{Te}$ -

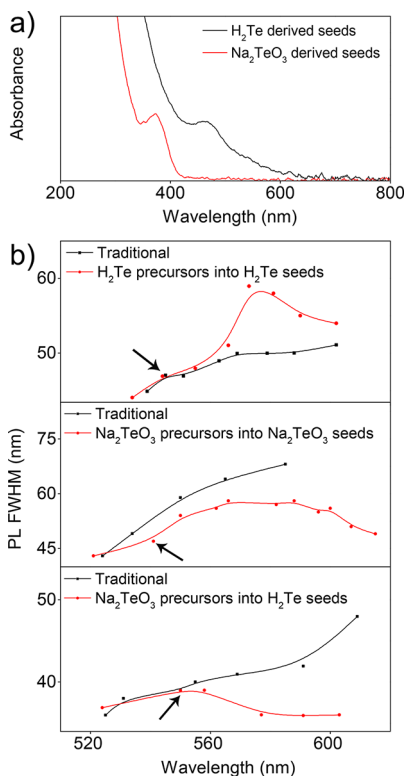


**Figure 6.** Comparison of different combinations of precursors and seeds used in PDPA syntheses. (a) Absorption spectra of the two different Te precursor systems:  $\text{H}_2\text{Te}$ -derived seeds and  $\text{Na}_2\text{TeO}_3$ -derived seeds. (b) Trends for the PL fwhm of three different systems (from top to bottom):  $\text{H}_2\text{Te}$  precursors injected into  $\text{H}_2\text{Te}$ -derived seeds;  $\text{Na}_2\text{TeO}_3$  precursors injected into  $\text{Na}_2\text{TeO}_3$ -derived seeds; and  $\text{Na}_2\text{TeO}_3$  precursors injected into the  $\text{H}_2\text{Te}$ -derived seeds. The black arrows in the top to bottom figures indicate the PDPA starting point.

derived CdTe seeds show an excitonic peak at 480 nm and are larger than those formed in the  $\text{Na}_2\text{TeO}_3$  system with the corresponding peak at 390 nm. In one control experiment, additional QD precursor sources provided by the  $\text{H}_2\text{Te}$  precursor instead of  $\text{Na}_2\text{TeO}_3$  were introduced into the  $\text{H}_2\text{Te}$ -derived seed system, as shown in Figure 6b (top), where the remaining reaction parameters between the additional precursor source and seed systems were identical. It is obvious that the fwhm increased immediately after the  $\text{H}_2\text{Te}$ -grown system was used as the PDPA precursor source with the  $\text{H}_2\text{Te}$  grown seeds. It can be rationalized that the additional precursor source QDs are large and do not redissolve so readily in the refluxing solution. After injection into the reaction mixture, the newcomers therefore tend to ripen and grow independently of the seed population, leading to a larger

polydispersity of the resulting QDs. From this, we conclude that the added precursors should not be too large in comparison with the seed size distribution.

In another control experiment, as shown in Figure 6b (middle), the starting seeds were  $\text{Na}_2\text{TeO}_3$ -derived seeds instead of the previous  $\text{H}_2\text{Te}$ -derived seeds, and meanwhile the additional precursor source QDs for PDPA were also provided by a  $\text{Na}_2\text{TeO}_3$  synthesis, where the reaction parameters (apart from reflux times) between the additional precursor and seed systems were identical. The  $\text{Na}_2\text{TeO}_3$ -derived replenisher injected as a precursor source into the  $\text{Na}_2\text{TeO}_3$  seed solution showed another distinct behavior. After the start of injection, the PL fwhm increased for a period of time and narrowed down later, as shown in Figure 6b (middle). We propose that the additional precursors are too small to grow rapidly as an independent population; they rather dissolve immediately after entering the reaction. This leads to a sudden large supply of additional precursors for already existing larger seeds, which fuels the growth of not only the larger particles but also smaller particles, in the starting ensemble. These newly formed QDs differ in sizes from the original particles, which causes an observed increase of the PL fwhm for a while. As the reaction progresses, the smaller QDs grow faster than the larger ones when entering the size-focusing regime, resulting in the gradual decrease in the PL fwhm. We thus conclude that the seeds should not be too small compared with the PDPA precursor.

Figure 6b (bottom) shows a third distinct case, where the  $\text{Na}_2\text{TeO}_3$ -derived precursor source was PDPA injected into the  $\text{H}_2\text{Te}$ -derived seeds, and afterward the PL fwhm decreased immediately. Compared with the first situation (Figure 6b, top), the PDPA precursors are small enough to dissolve easily (more readily than the seeds), so they do not start to contribute to the size distribution by growing themselves. Compared with the second situation (Figure 6b, middle), the seeds in the original solutions are bigger and will themselves consume the fresh precursors and hence avoid leaving an excess of the PDPA precursors available for fresh nucleation again. Thus, the major consumption of the PDPA precursors will be driving the enlargement of the particles in the ensemble. The comparison of three cases shows that it is of a primary importance to sensibly match the sizes of the PDPA precursors and the seed particles in order to be able to achieve size focusing and rapid growth whilst at the same time suppressing the Ostwald ripening.

**Effect of Precursor Source QD Size on Emission Peak Narrowing.** In order to figure out how the sizes of the seeds and the QD precursors influence the emission peak widths, we further extended the previous experiments. In a series of syntheses, the size of the PDPA precursor source QDs was varied from 2.0 nm (absorption peak position 415 nm) to 2.6 nm (absorption peak position 488 nm), all derived from the  $\text{Na}_2\text{TeO}_3$  system by heating the precursor solution for various times. The sizes were estimated from a sizing curve relationship shown alongside Table S2. These were introduced at 7.5 mL/h injection speed, into seed solutions derived from the  $\text{H}_2\text{Te}$  system (diameter 3.3 nm and absorption peak position 555 nm). Five different sized precursor source QDs were used, denoted as precursors 1–5, with absorption peaks at 415 nm (precursor 1), 432 nm (precursor 2), 451 nm (precursor 3), 475 nm (precursor 4), and 488 nm (precursor 5). The resulting PL fwhms strongly depend on the size of QD precursors (the left panel of Figure 7a), corresponding precursors absorption (the middle panel of Figure 7a), and PL spectra (the right panel

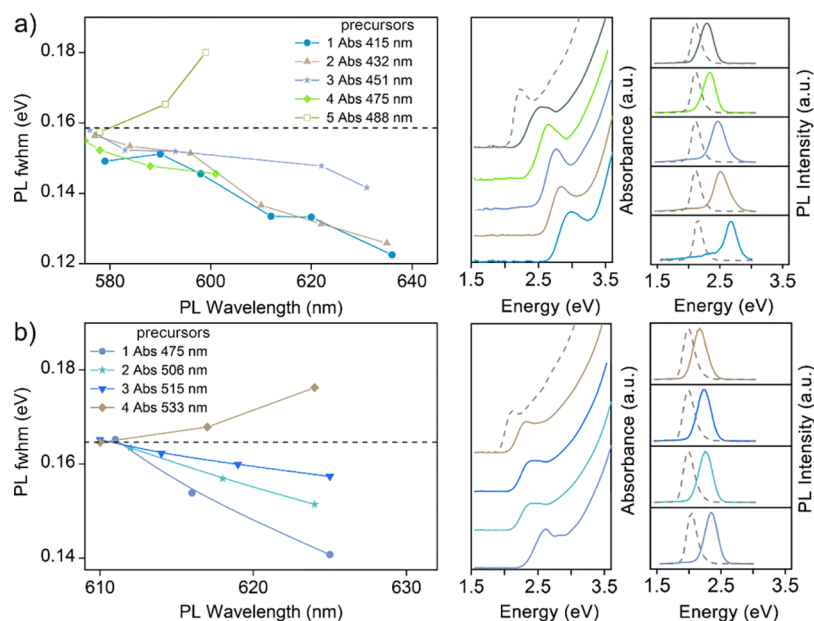


**Figure 7.** Effect on the PL fwhm of resulting CdTe QDs via PDPA method by using different sizes of QD precursors (the corresponding additional precursor absorbance spectra and PL spectra are shown in the middle and right, respectively), together with the two seeds (dashed lines) which were derived from  $\text{H}_2\text{Te}$ : (a) 3.3 nm diameter, absorption peak position 555 nm (dashed lines). (b) 3.7 nm diameter, absorption peak position 586 nm (dashed lines).

of Figure 7a). Only for the largest seeds with the absorption peak at 488 nm, was the resulting size distribution of the QDs significantly broadened. We note that the distinction between the seed sizes that lead to either broadening or narrowing of the ensemble size distribution is rather fine. Precursor 4 with a mean diameter of 2.4 nm (absorption peak position 475 nm) exhibited PL narrowing, whereas precursor 5, marginally larger at 2.6 nm (absorption peak position 488 nm), caused PL broadening. Similar QD precursor size dependences were also observed for larger QD seeds (3.7 nm, absorption peak position 586 nm), as shown in Figure 7b, where different sized precursor source QDs were used ranging from 2.4 nm (absorption peak position 475 nm) to 3.0 nm (absorption peak position 533 nm). Here, the PDPA rate was reduced to 2.5 mL/h because as the seeds become bigger, QD growth significantly slows down so that the injection speed needs to be reduced accordingly.

The findings from the above experiments suggest that irrespective of the type of precursors used to grow the precursor source QDs and seed QDs or their respective sizes, the critical factor that determines if the size distribution of particles in the final QD ensemble will become broad or narrow is the precursor source QD lability, that is, its ability to undergo rapid enough redissolution relative to that of the seed particles, and also the demand for precursor in the seed solution. If precursors are significantly oversized relative to the seeds, they cannot release the necessary precursor rapidly enough; instead in a dynamic equilibrium, they will consume any redissolved precursor themselves. In the other extreme, if the sizes of the QD precursors and seeds are too close to be clearly distinguished from each other, the seed solution cannot digest such an influx of material from the added precursor, and the seed and the precursor populations tend to grow alongside each other indistinguishably.

## CONCLUSIONS

We have introduced a synthesis approach which we denote as programmed dropwise precursor (source) addition (PDPA) to obtain a series of aqueously grown CdTe QDs, which experienced remarkable monodispersity and, as a result, narrow PL peaks, over a wide range of emission wavelengths. In order to precisely control the precursor supply speed and the volume of the injected solution, a programmable syringe pump was used. This allowed us to explore the particle growth rates and the size dispersion dependence upon the timing and injecting volumes used in the precursor source addition. By carefully timing the point at which a precursor solution is added during reflux, we can switch from the Ostwald ripening regime to diffusion-limited growth, which result in the size focusing of QDs. By applying the PDPA method, we replenished the precursors before size defocusing occurred and thus restrained the Ostwald ripening process successfully. In this manner, the PL fwhm of CdTe QDs in the red spectral region was as narrow as 106 meV, which was even narrower than that for PL spectra in the green region (160 nm). Furthermore, we introduced monitoring of the solution conductivity to track the consumption of precursors furnished by the injected QDs during the ongoing reaction, which provided us with valuable feedback as to whether the PDPA volume and injection timing were appropriate. Moreover, supplying precursors at a too high rate was seen to decrease the PL QY of the resulting QDs, whereas adopting a proper supply rate was found to maintain the high initial PL QY at an almost constant level. Likewise, we found that the proper adjustment of the precursor supply tends to increase the radiative recombination lifetimes and thus lengthen PL lifetimes. If radiative lifetimes are increased but the PL QY is (nearly) maintained in the best cases, then the nonradiative recombination rates are most likely also being reduced at the same time, which may indicate improved surface quality. We also found the best combination of precursor source QDs and seeds for size focusing to be smaller precursor

QDs synthesized using  $\text{Na}_2\text{TeO}_3$  injected into larger seed particle solutions grown using the  $\text{H}_2\text{Te}$  precursor. These experiments further demonstrated that size focusing depends on the precursor source QD reaction lability and the precursor demand in the seed solution.

## ■ ASSOCIATED CONTENT

### 📄 Supporting Information

The Supporting Information is available free of charge on the ACS Publications website at DOI: 10.1021/acs.jpcc.8b01053.

Particle size histograms from TEM images of CdTe QDs; relationship between fwhm and conductivity in the solution, a blank experiment of  $\text{NaBH}_4$  conductivity variation during refluxing at 100 °C under open-air conditions with condenser attached; EDS data of CdTe QDs and the relative ratio of Cd/Te and S/Te in the particles synthesized by traditional and PDPA methods; comparison of the absorption spectra of traditional synthesis and PDPA-synthesized CdTe QDs; detailed fitting processes for PL decay curves and tabulated fitting parameters; and absorption peak position and calculation of the dimensions of seeds and PDPA precursors in Figure 7 (PDF)

## ■ AUTHOR INFORMATION

### Corresponding Authors

\*E-mail: jinglh@iccas.ac.cn (L.J.).

\*E-mail: andrey.rogach@cityu.edu.hk (A.L.R.).

\*E-mail: gaomy@iccas.ac.cn (M.G.).

### ORCID

Stephen V. Kershaw: 0000-0003-0408-4902

Andrey L. Rogach: 0000-0002-8263-8141

Mingyuan Gao: 0000-0002-7360-3684

### Author Contributions

The manuscript was written through contributions of all authors. All authors have given approval to the final version of the manuscript.

### Notes

The authors declare no competing financial interest.

## ■ ACKNOWLEDGMENTS

Funding has been provided by the National Natural Science Foundation of China (81671755, 21203210, 81530057), and the Research Grant Council of Hong Kong SAR (CityU 11302114).

## ■ REFERENCES

- (1) Mashford, B. S.; Stevenson, M.; Popovic, Z.; Hamilton, C.; Zhou, Z.; Breen, C.; Steckel, J.; Bulovic, V.; Bawendi, M.; Coe-Sullivan, S. High-efficiency quantum-dot light-emitting devices with enhanced charge injection. *Nat. Photonics* **2013**, *7*, 407–412.
- (2) Jing, L.; Kershaw, S. V.; Li, Y.; Huang, X.; Li, Y.; Rogach, A. L.; Gao, M. Aqueous Based Semiconductor Nanocrystals. *Chem. Rev.* **2016**, *116*, 10623–10730.
- (3) Kershaw, S. V.; Jing, L.; Huang, X.; Gao, M.; Rogach, A. L. Materials aspects of semiconductor nanocrystals for optoelectronic applications. *Mater. Horiz.* **2017**, *4*, 155–205.
- (4) Bruchez, M.; Moronne, M.; Gin, P.; Weiss, S.; Alivisatos, A. P. Semiconductor nanocrystals as fluorescent biological labels. *Science* **1998**, *281*, 2013–2016.
- (5) Chan, W. C. W.; Nie, S. Quantum dot bioconjugates for ultrasensitive nonisotopic detection. *Science* **1998**, *281*, 2016–2018.

(6) Dubertret, B.; Skourides, P.; Norris, D. J.; Noireaux, V.; Brivanlou, A. H.; Libchaber, A. In vivo imaging of quantum dots encapsulated in phospholipid micelles. *Science* **2002**, *298*, 1759–1762.

(7) McHugh, K. J.; Jing, L. H.; Behrens, A. M.; Jayawardena, H. S. N.; Tang, W.; Gao, M. Y.; Langer, R.; Jaklenc, A. Biocompatible Semiconductor Quantum Dots as Cancer Imaging Agents. *Adv. Mater.* **2018**, *30*, 1706356.

(8) Pradhan, N.; Battaglia, D. M.; Liu, Y.; Peng, X. Efficient, stable, small, and water-soluble doped ZnSe nanocrystal emitters as non-cadmium biomedical labels. *Nano Lett.* **2007**, *7*, 312–317.

(9) Winter, J. O.; Liu, T. Y.; Korgel, B. A.; Schmidt, C. E. Recognition molecule directed interfacing between semiconductor quantum dots and nerve cells. *Adv. Mater.* **2001**, *13*, 1673–1677.

(10) Panthani, M. G.; Khan, T. A.; Reid, D. K.; Hellebusch, D. J.; Rasch, M. R.; Maynard, J. A.; Korgel, B. A. In Vivo Whole Animal Fluorescence Imaging of a Microparticle-Based Oral Vaccine Containing (CuInSe<sub>x</sub>S<sub>2-x</sub>)/ZnS Core/Shell Quantum Dots. *Nano Lett.* **2013**, *13*, 4294–4298.

(11) Gao, M.; Kirstein, S.; Möhwald, H.; Rogach, A. L.; Kornowski, A.; Eychmüller, A.; Weller, H. Strongly photoluminescent CdTe nanocrystals by proper surface modification. *J. Phys. Chem. B* **1998**, *102*, 8360–8363.

(12) Rogach, A. L.; Katsikas, L.; Kornowski, A.; Su, D.; Eychmüller, A.; Weller, H. Synthesis, morphology and optical properties of thiol-stabilized CdTe nanoclusters in aqueous solution. *Ber. Bunsen-Ges. Phys. Chem.* **1997**, *101*, 1668–1670.

(13) Zhang, H.; Zhou, Z.; Yang, B.; Gao, M. The influence of carboxyl groups on the photoluminescence of mercaptocarboxylic acid-stabilized CdTe nanoparticles. *J. Phys. Chem. B* **2003**, *107*, 8–13.

(14) Bao, H.; Gong, Y.; Li, Z.; Gao, M. Enhancement effect of illumination on the photoluminescence of water-soluble CdTe nanocrystals: Toward highly fluorescent CdTe/CdS core-shell structure. *Chem. Mater.* **2004**, *16*, 3853–3859.

(15) Nabiev, I.; Mitchell, S.; Davies, A.; Williams, Y.; Kelleher, D.; Moore, R.; Gun'ko, Y. K.; Byrne, S.; Rakovich, Y. P.; Donegan, J. F. Nonfunctionalized nanocrystals can exploit a cell's active transport machinery delivering them to specific nuclear and cytoplasmic compartments. *Nano Lett.* **2007**, *7*, 3452–3461.

(16) Zintchenko, A.; Susha, A. S.; Concia, M.; Feldmann, J.; Wagner, E.; Rogach, A. L.; Ogris, M. Drug Nanocarriers Labeled With Near-infrared-emitting Quantum Dots (Quantoplexes): Imaging Fast Dynamics of Distribution in Living Animals. *Mol. Ther.* **2009**, *17*, 1849–1856.

(17) Deka, S.; Quarta, A.; Lupo, M. G.; Falqui, A.; Boninelli, S.; Giannini, C.; Morello, G.; De Giorgi, M.; Lanzani, G.; Spinella, C. CdSe/CdS/ZnS Double Shell Nanorods with High Photoluminescence Efficiency and Their Exploitation As Biolabeling Probes. *J. Am. Chem. Soc.* **2009**, *131*, 2948–2958.

(18) Biju, V.; Itoh, T.; Ishikawa, M. Delivering quantum dots to cells: bioconjugated quantum dots for targeted and nonspecific extracellular and intracellular imaging. *Chem. Soc. Rev.* **2010**, *39*, 3031–3056.

(19) Li, Y.; Duan, X.; Jing, L.; Yang, C.; Qiao, R.; Gao, M. Quantum dot-antisense oligonucleotide conjugates for multifunctional gene transfection, mRNA regulation, and tracking of biological processes. *Biomaterials* **2011**, *32*, 1923–1931.

(20) Tang, Z.; Zhang, Z.; Wang, Y.; Glotzer, S. C.; Kotov, N. A. Self-Assembly of CdTe Nanocrystals into Free-Floating Sheets. *Science* **2006**, *314*, 274–278.

(21) Yeom, J.; Yeom, B.; Chan, H.; Smith, K. W.; Dominguez-Medina, S.; Bahng, J. H.; Zhao, G.; Chang, W.-S.; Chang, S.-J.; Chuvilin, A. Chiral templating of self-assembling nanostructures by circularly polarized light. *Nat. Mater.* **2015**, *14*, 66–72.

(22) Zhou, Y.; Yang, M.; Sun, K.; Tang, Z.; Kotov, N. A. Similar Topological Origin of Chiral Centers in Organic and Nanoscale Inorganic Structures: Effect of Stabilizer Chirality on Optical Isomerism and Growth of CdTe Nanocrystals. *J. Am. Chem. Soc.* **2010**, *132*, 6006–6013.

- (23) Ma, W.; Xu, L.; de Moura, A. F.; Wu, X.; Kuang, H.; Xu, C.; Kotov, N. A. Chiral Inorganic Nanostructures. *Chem. Rev.* **2017**, *117*, 8041–8093.
- (24) Yan, W.; Xu, L.; Xu, C.; Ma, W.; Kuang, H.; Wang, L.; Kotov, N. Self-Assembly of Chiral Nanoparticle Pyramids with Strong R/S Optical Activity. *J. Am. Chem. Soc.* **2012**, *134*, 15114–15121.
- (25) Zhang, H.; Cui, Z.; Wang, Y.; Zhang, K.; Ji, X.; Lü, C.; Yang, B.; Gao, M. From water-soluble CdTe nanocrystals to fluorescent nanocrystal-polymer transparent composites using polymerizable surfactants. *Adv. Mater.* **2003**, *15*, 777–780.
- (26) Guo, J.; Yang, W.; Wang, C. Systematic study of the photoluminescence dependence of thiol-capped CdTe nanocrystals on the reaction conditions. *J. Phys. Chem. B* **2005**, *109*, 17467–17473.
- (27) Zhang, H.; Wang, L.; Xiong, H.; Hu, L.; Yang, B.; Li, W. Hydrothermal synthesis for high-quality CdTe nanocrystals. *Adv. Mater.* **2003**, *15*, 1712.
- (28) He, Y.; Sai, L.-M.; Lu, H.-T.; Hu, M.; Lai, W.-Y.; Fan, Q.-L.; Wang, L.-H.; Huang, W. Microwave-assisted synthesis of water-dispersed CdTe nanocrystals with high luminescent efficiency and narrow size distribution. *Chem. Mater.* **2007**, *19*, 359–365.
- (29) Rogach, A. L.; Franzl, T.; Klar, T. A.; Feldmann, J.; Gaponik, N.; Lesnyak, V.; Shavel, A.; Eychmüller, A.; Rakovich, Y. P.; Donegan, J. F. Aqueous synthesis of thiol-capped CdTe nanocrystals: State-of-the-art. *J. Phys. Chem. C* **2007**, *111*, 14628–14637.
- (30) Zou, L.; Gu, Z.; Zhang, N.; Zhang, Y.; Fang, Z.; Zhu, W.; Zhong, X. Ultrafast synthesis of highly luminescent green- to near infrared-emitting CdTe nanocrystals in aqueous phase. *J. Mater. Chem.* **2008**, *18*, 2807–2815.
- (31) Zhou, D.; Zou, H.; Liu, M.; Zhang, K.; Sheng, Y.; Cui, J.; Zhang, H.; Yang, B. Surface Ligand Dynamics-Guided Preparation of Quantum Dots Cellulose Composites for Light-Emitting Diodes. *ACS Appl. Mater. Interfaces* **2015**, *7*, 15830–15839.
- (32) Murray, C. B.; Norris, D. J.; Bawendi, M. G. Synthesis and characterization of nearly monodisperse CdE (E = sulfur, selenium, tellurium) semiconductor nanocrystallites. *J. Am. Chem. Soc.* **1993**, *115*, 8706–8715.
- (33) Peng, X.; Schlamp, M. C.; Kadavanich, A. V.; Alivisatos, A. P. Epitaxial growth of highly luminescent CdSe/CdS core/shell nanocrystals with photostability and electronic accessibility. *J. Am. Chem. Soc.* **1997**, *119*, 7019–7029.
- (34) Park, J.; Joo, J.; Kwon, S. G.; Jang, Y.; Hyeon, T. Synthesis of monodisperse spherical nanocrystals. *Angew. Chem., Int. Ed.* **2007**, *46*, 4630–4660.
- (35) Peng, X.; Wickham, J.; Alivisatos, A. P. Kinetics of II-VI and III-V colloidal semiconductor nanocrystal growth: "Focusing" of size distributions. *J. Am. Chem. Soc.* **1998**, *120*, 5343–5344.
- (36) Franke, D.; Harris, D. K.; Chen, O.; Bruns, O. T.; Carr, J. A.; Wilson, M. W. B.; Bawendi, M. G. Continuous injection synthesis of indium arsenide quantum dots emissive in the short-wavelength infrared. *Nat. Commun.* **2016**, *7*, 12749.
- (37) Tamang, S.; Lee, S.; Choi, H.; Jeong, S. Tuning Size and Size Distribution of Colloidal InAs Nanocrystals via Continuous Supply of Prenucleation Clusters on Nanocrystal Seeds. *Chem. Mater.* **2016**, *28*, 8119–8122.
- (38) Gaponik, N.; Talapin, D. V.; Rogach, A. L.; Hoppe, K.; Shevchenko, E. V.; Kornowski, A.; Eychmüller, A.; Weller, H. Thiol-capping of CdTe nanocrystals: An alternative to organometallic synthetic routes. *J. Phys. Chem. B* **2002**, *106*, 7177–7185.
- (39) Shavel, A.; Gaponik, N.; Eychmüller, A. Factors Governing the Quality of Aqueous CdTe Nanocrystals: Calculations and Experiment. *J. Phys. Chem. B* **2006**, *110*, 19280–19284.
- (40) Jing, L.; Kershaw, S. V.; Kipp, T.; Kalytchuk, S.; Ding, K.; Zeng, J.; Jiao, M.; Sun, X.; Mews, A.; Rogach, A. L.; et al. Insight into Strain Effects on Band Alignment Shifts, Carrier Localization and Recombination Kinetics in CdTe/CdS Core/Shell Quantum Dots. *J. Am. Chem. Soc.* **2015**, *137*, 2073–2084.
- (41) Yang, Y.; Wen, Z.; Dong, Y.; Gao, M. Incorporating CdTe nanocrystals into polystyrene microspheres: Towards robust fluorescent beads. *Small* **2006**, *2*, 898–901.
- (42) Talapin, D. V.; Rogach, A. L.; Haase, M.; Weller, H. Evolution of an ensemble of nanoparticles in a colloidal solution: Theoretical study. *J. Phys. Chem. B* **2001**, *105*, 12278–12285.
- (43) Bao, H.; Wang, E.; Dong, S. One-pot synthesis of CdTe nanocrystals and shape control of luminescent CdTe-cystine nanocomposites. *Small* **2006**, *2*, 476–480.
- (44) Kamal, J. S.; Omari, A.; Van Hoecke, K.; Zhao, Q.; Vantomme, A.; Vanhaecke, F.; Capek, R. K.; Hens, Z. Size-Dependent Optical Properties of Zinc Blende Cadmium Telluride Quantum Dots. *J. Phys. Chem. C* **2012**, *116*, 5049–5054.
- (45) Jasieniak, J.; Mulvaney, P. From Cd-rich to Se-rich - The manipulation of CdSe nanocrystal surface stoichiometry. *J. Am. Chem. Soc.* **2007**, *129*, 2841–2848.
- (46) Petkov, V.; Moreels, I.; Hens, Z.; Ren, Y. PbSe quantum dots: Finite, off-stoichiometric, and structurally distorted. *Phys. Rev. B: Condens. Matter Mater. Phys.* **2010**, *81*, 241304.
- (47) Smith, A. M.; Lane, L. A.; Nie, S. Mapping the spatial distribution of charge carriers in quantum-confined heterostructures. *Nat. Commun.* **2014**, *5*, 4506.
- (48) Kershaw, S. V.; Abdelazim, N. M.; Zhao, Y.; Susha, A. S.; Zhovtiuk, O.; Teoh, W. Y.; Rogach, A. L. Investigation of the Exchange Kinetics and Surface Recovery of Cd<sub>x</sub>Hg<sub>1-x</sub>Te Quantum Dots during Cation Exchange Using a Microfluidic Flow Reactor. *Chem. Mater.* **2017**, *29*, 2756–2768.
- (49) Marple, D. T. F. Refractive index of ZnSe, ZnTe, CdTe. *J. Appl. Phys.* **1964**, *35*, 539.
- (50) Moreels, I.; Lambert, K.; De Muynck, D.; Vanhaecke, F.; Poelman, D.; Martins, J. C.; Allan, G.; Hens, Z. Composition and size-dependent extinction coefficient of colloidal PbSe quantum dots. *Chem. Mater.* **2007**, *19*, 6101–6106.
- (51) Lenham, A. P.; Treherne, D. M. Optical constants of single crystals of cadmium + zinc. *Proc. Phys. Soc. Lond.* **1964**, *83*, 1059.
- (52) Neeves, A. E.; Birnboim, M. H. Composite structures for the enhancement of nonlinear-optical susceptibility. *J. Opt. Soc. Am. B* **1989**, *6*, 787–796.
- (53) Hens, Z.; Moreels, I. Light absorption by colloidal semiconductor quantum dots. *J. Mater. Chem.* **2012**, *22*, 10406–10415.
- (54) Delerue, C.; Lannoo, M.; Allan, G. Concept of dielectric constant for nanosized systems. *Phys. Rev. B: Condens. Matter Mater. Phys.* **2003**, *68*, 115411.
- (55) Franceschetti, A. Structural and electronic properties of PbSe nanocrystals from first principles. *Phys. Rev. B: Condens. Matter Mater. Phys.* **2008**, *78*, 075418.